Published in final edited form as:
Biochemistry. 2013 January 15; 52(2): 415–424. doi:10.1021/bi301492j.

The Gate that Governs Sulfotransferase Selectivity

Ian Cook[1], **Ting Wang**[1], **Steven C. Almo**[2], **Jungwook Kim**[2], **Charles N. Falany**[3], and **Thomas S. Leyh**[1,3,*]

[1]Department of Microbiology and Immunology, Albert Einstein College of Medicine, 1300 Morris Park Ave, Bronx, New York 10461-1926

[2]Department of Biochemistry, Albert Einstein College of Medicine, 1300 Morris Park Ave, Bronx, New York 10461-1926

[3]Pharmacology and Toxicology, University of Alabama School of Medicine at Birmingham, 1670 University Boulevard, VH 151, Birmingham, Al 35294-0019

Abstract

Human cytosolic sulfotransferases (SULTs) transfer the sulfuryl-moiety (-SO_3) from activated sulfate (3′-phosphoadenosine 5′-phosphosulfate, PAPS) to the hydroxyls and primary amines of numerous metabolites, drugs and xenobiotics. Receipt of the sulfuryl-group often radically alters acceptor-target interactions. How these enzymes select particular substrates from the hundreds of candidates in a complex cytosol remains an important question. Recent work reveals PAPS binding causes SULT2A1to undergo an isomerization that controls selectivity by constricting the opening through which acceptors must pass to enter the active site. The enzyme maintains an affinity for large substrates by isomerizing between the open and closed states with nucleotide bound. Here, the molecular basis of the nucleotide-induced closure is explored in equilibrium and non-equilibrium molecular dynamics simulations. The simulations predict that the active-site "cap," which covers both the nucleotide and acceptor binding sites, opens and closes in response to nucleotide. The cap subdivides into nucleotide and acceptor halves whose motions, while coupled, exhibit an independence that can explain the isomerization. *In-silico* weakening of electrostatic interactions between the cap and base of the active site causes the acceptor-half of the cap to open and close while the nucleotide lid remains shut. Simulations predict that SULT1A1, the most abundant SULT in human liver, will utilize a similar selection mechanism. This prediction is tested using fulvestrant, an antiestrogen too large to pass through the closed pore, and estradiol, which is not restricted by closure. Equilibrium and presteady state binding studies confirm that SULT1A1 undergoes a nucleotide induced isomerzation that controls substrate selection.

Keywords

sulfotransferase; SULT; SULT1A1; SULT2A1; fulvestrant; estradiol; kinetic; mechanism; ligand; binding; presteady; fluorescence; structure; selection; substrate; GROMACS; molecular dynamics

Human cytosolic sulfotransferases play a critical role in regulating metabolism. These enzymes transfer the sulfury-moiety from the donor, activated sulfate (1), to the hydroxyls and primary amines of hundreds if not thousands of acceptors. Sulfonation often profoundly alters the affinities of compounds for their targets, which include nuclear (2–4) and dopamine receptors (5). Sulfatases, which remove the sulfuryl-group, counterbalance the

*Corresponding Author: The Department Microbiology and Immunology, Albert Einstein College of Medicine, 1300 Morris Park Ave., Bronx, New York 10461-1926, Phone: 718-430-2857, Fax: 718-430-8711, leyh@einstein.yu.edu.

activities of sulfotransferases and their combined actions determine the *in-vivo* activities of many biomolecules (6). Primary roles of sulfotransferases include regulating the activities of signaling small molecules (2–5) and defending receptors from perturbations caused by the binding of xenobiotics that resemble signaling molecule (7, 8). These homeostatic and defensive functions place very different demands on selectivity. The former requires that SULTs operate on a cohort of related structures; the latter requires them to act on a much broader set of structures whose common element is a resemblance to the receptor-binding features of the cohort. The molecular mechanism that underlies this dual-specificity in the human SULTs 1A1 and 2A1 is the focus of this work.

SULTs 1A1 and 2A1 are found in numerous tissues and are concentrated in liver, where they are found in gram quantities, 0.9 and 0.3 g/kg wet weight, respectively (7, 9)). The substrate spectrum of SULT1A1 is the broadest of any SULT (1, 10, 11). Its substrates include small planar molecules (12), steroids (13), cyclic amines (14), numerous drugs (10, 15–17) and small peptides (18). The spectrum of SULT2A1, while broad by many standards (19–22), centers on steroid-like structures, for which it exhibits substantially higher affinities than SULT1A1 (23). Together, these enzymes comprise ~ 90% of sulfotransferases in liver and are a significant means of homeostatic balance and detoxication in the human body (7).

The binding of nucleotide causes an isomerization that restricts access to the acceptor-binding pocket of SULT2A1 (24). Structures with and without nucleotide bound suggest that the restriction is due to a repositioning of a nine-reside segment located at the entrance to the acceptor-binding pocket. This molecular “gate” forms part of the active site “cap,” which covers both the nucleotide and acceptor binding sites and is conserved in the family. Protein-function work has shown that the enzyme isomerizes between gate- “open” and “closed” states while nucleotide remains bound. Active-site access to compounds small enough to pass through the restricted opening is not affected by the position of the gate. Substrates too large to pass though the opening can bind only when the gate has “swung” to the open position. Thus, large-substrate access is controlled by the equilibrium constant that governs the isomerization, K_{iso}. The selectivity’s of the open and closed forms appear well suited to the dual-specificity demands placed on these enzymes (24).

The current work explores the molecular basis of the gating mechanism through computation and experiment. Equilibrium and non-equilibrium molecular dynamics simulations suggest molecular details of how the cap disengages from the base of the active site, and that a considerable increase in dynamics occurs when the gate opens. Remarkably, the modeling predicts an isomerization in which the “acceptor-half” of the cap can “peel” away from the base while leaving the nucleotide-half closed. Gating has not been tested in SULT1A1. The models suggest that gating occurs in 1A1 and this prediction is born out in equilibrium and presteady-state binding studies. The metabolic utility of the gating mechanism is discussed in the context of the environment in which these enzymes are expressed, the hepatocyte cytosol (9, 25).

Materials and Methods

The materials and their sources are as follows: dithiothreitol (DTT), EDTA, L-glutathione (reduced, GSH), glucose, imidazole, isopropyl-thio-β-D-galactopyranoside (ITPG), LB media, lysozyme, β-mercaptoethanol, pepstatin A, fulvestrant, estradiol (E2) and potassium phosphate were the highest grade available from Sigma. Ampicillin, HEPES, KOH, $MgCl_2$, NaCl, KCl, and phenylmethylsulfonyl fluoride were purchased from Fisher Scientific. Glutathione- and nickel-chelating resins were obtained from GE Healthcare. Competent *E. coli* (BL21(DE3)) was purchased from Novagen. PAP and PAPS were enzymatically

synthesized as previously described (3, 26). PAPS purity was ≥ 98% as assessed by anion-exchange HPLC.

Protein Purification

Human SULT1A1 DNA was codon optimized for *E. coli* (MR. GENE, Germany) and inserted into a triple-tag pGEX-6P expression vector with an N-terminal His/GST/MBP tag (24, 26). The plasmid was transfected into *E. coli* (BL-21(DE3)) and SULT1A1 was expressed and purified as described previously (24, 26). Briefly, the cell pellet was suspended in lysis buffer, sonicated, and centrifuged. The supernatant was loaded onto a Chelating Sepharose Fast Flow column charged with Ni^{2+}. The fusion protein was eluted with imidazole (250 mM) onto a Glutathione Sepharose column and then eluted using GSH (10 mM). The fusion protein was digested with Precision Protease and dialyzed overnight against HEPES/K^+ (50 mM, pH = 7.5), DTT (1.5 mM), KCl (50 mM) at 4 °C. The sample was passed back through the glutathione column to remove the tag. SULT1A1 was concentrated using a 10 kDa cutoff filter and stored at −80 °C in 40% glycerol. Protein purity was assessed at > 97% using SDS PAGE. Protein concentration was determined spectrophotometrically (ε_{280} = 36.7 mM^{-1} cm^{-1}) (3).

Crystallization and Structure Determination

The SULT1A1· PAP complex was formed by addition of PAP (0.50 mM) to protein at 15mg/mL. The complex was crystallized by sitting drop vapor diffusion at 21°C by mixing 1.0 μL of the protein with 1.0 μL of reservoir solution (Tris (0.10 M, pH 8.0), PEG (20%) and 1,3-butanediol (4% v/v)) and equilibrating over 0.10 mL of reservoir solution. Crystals were transferred to reservoir solution supplemented with 20% glycerol prior to flash-cooling in liquid nitrogen. X-ray data were collected on an ADSC QUANTUM 315 CCD detector at the NSLS beam line X29A and processed with HKL3000 (27). Diffraction data from a ligand-bound SULT crystal were collected at wavelength λ = 1.075 nm and were consistent with space group $P2_1$ (a = 48.44, b = 122.63, c = 55.00Å; β = 91.46) with two molecules per asymmetric unit. Due to the high degree of anisotropy of the diffraction data the *'Use Auto Corrections'* function of the HKL3000 program was used during scaling, and the resolution was limited to 2.60 Å from 2.30 Å. Molecular replacement was performed using the PAP-bound SULT structure (pdb code 2D06) as a search model with MOLREP (28). Subsequent model building and refinement was performed with Coot (29) and REFMAC5 (28). The final model was refined to 2.60 Å with R_{work} = 0.214 and R_{free} = 0.266.

Software and Computational Equipment

The simulations were performed on a Parallel Quantum Solutions QS32-2670C-XS8 computer. MODELLER was provided by the University of California, San Francisco. A GOLD license was obtained from the Cambridge Crystallographic Data Center. The source code for GROMACS 4.5 was downloaded from http://www.GROMACS.org under the GROMCAS General Public License (GPL). AMBER and Ambertools 10.0 were obtained from the University of California, San Francisco.

Molecular Dynamic Simulations

Models of SULT2A1 were constructed from the available binary crystal structure of SULT2A1 and PAP (1EFH) (30). SULT1A1 models were constructed using the SULT1A1·PAP structure determined in this study (4GRA). Missing atoms were added using MODELER (31). The protein was solvated using approximately 3000 SPC water (32) molecules in a cube large enough to allow at least 1.0 nm of water between protein and cube surfaces (33). For simulations involving PAPS-bound enzyme, the PAPS structure was obtained from the SULT1E1·PAPS structure (PDB 1HY3) (34). The PAPS charge

distribution was calculated using AmberTools 10.0 (35) and PAP was replaced with PAPS in the crystal structure. The net charge of the system was balanced with Na^+, and NaCl was added to the box to a simulated concentration of 0.15 M (33). Non-covalent interactions were cut off at 1.0 nm. STEEPEST DECENTS in GROMACS was used to energy minimize the system (36). Once minimized, the protein-solvent system was heated to a simulated temperature of 310K and the system was then stabilized using Berendsen temperature and pressure coupling (37, 38). Bonds were constrained with LINCS (39). The simulation was then run for 1.0 nsec. A time step of 2 fs was used through the warming and simulation steps and structures were written every 0.5 ps. RMSD values were then plotted *vs.* time to determine whether the system had reached equilibrium. Once equilibrated, the simulation was run for 10 nsec. All analyses were performed after equilibration using programs in GROMACS and VMD (33, 40). Mutants were generated by replacing target residues with glycine or serine. If necessary, the ion concentration was adjusted to maintain neutrality. Following R-group substitution, solvent was allowed to reorganize around the protein for 100 ps. Sixteen 1.0 ns simulations were then run in parallel. The key interaction distances were then averaged and plotted *vs* time. It should be noted that identical behaviors were observed when simulations were performed with monomers or dimers constructed using the canonical interface. Consequently, all simulations were performed using monomer structures.

In-Silico Docking

The SULT1A1·PAPS model used in ligand docking studies was developed from our SULT1A1·PAP structure (4GRA) as describe above, the unliganded (open) model of SULT1A1 was generated from the SULT1A1 simulations at equilibrium (see above) using the *g_cluster* function in GROMACS (41). Models were protonated and energy minimized using GOLD (42). Ligands were docked to the models using the Lamarckian evolution-based algorithm (43). After 250 simulated generations, the lowest energy orientation was saved for analysis. The algorithm was repeated 10 times for each combination of ligand and protein (43). A docking simulation was considered competent if the Gibbs binding potential was favorable and the nucleophilic hydroxyl of the ligand was within hydrogen bonding distance of the universally conserved, active-site histidine general base (44).

Equilibrium Binding of Fulvestrant and E2 to SULT1A1

Acceptor binding to SULT1A1 with or without bound nucleotide results in a substantial (20 – 40 %) decrease in the intrinsic fluorescence of the enzyme. Binding was monitored by fluorescence changes using a Carry Eclipse spectrometer, λ_{ex} = 290 nm, λ_{em} = 345 nm, 5 nm slit width. E2 and fulvestrant were titrated to a solution of SULT1A1 (10 nM, subunits), PAP (0 or 125 μM), $MgCl_2$ (5.0 mM), K_2PO_4 (25 mM), pH 7.4, 25 ± 2 °C. Titrations were performed by addition of concentrated ligand in ethanol:water vehicle (1:1 v/v). The total volume change was < 2.0 % and the final ethanol concentration was < 0.5%. Ethanol alone at 0.5% did not cause a change in fluorescence. Titrations were performed in triplicate. Data were averaged and least-squares fit using a model that assumes a single binding site *per* monomer (24, 26).

The binding algebra

The model used in fitting the equilibrium-binding titrations (Fig 5) is given in equation 1, which represents the gating mechanism under conditions where enzyme is saturated with nucleotide, a condition that holds for the binding studies ([nucleotide] > 15 × K_d in all titrations). The model includes an isomerzation that interconverts E′ and E, and a ligand-binding step in which ligand, L, can bind only to E. Given conservation of mass (eq. 2), the EL concentration can be expressed in terms of the concentration of solution-phase ligand, L, and an apparent binding constant, K_A, which is given by $K_d \cdot (1 + 1/K_{iso})$. Note that K_A ~

K_d when $K_{iso} \gg 1$. As a practical matter, L can be set equal to the concentration of total ligand, because < 4 % of ligand is enzyme bound at any point in the titrations. Binding is measured by following the change in intrinsic fluorescence of the enzyme. The fraction of bound enzyme (EL/E_T) at a particular ligand concentration is given by the change in fluorescence at that concentration (ΔI) divided by the change at saturating ligand (ΔI_{max}), $EL/E_T = \Delta I/\Delta I_{max}$. Estimates of K_A were obtained by least-squares fitting of the quadratic formula to the $\Delta I/\Delta I_{max}$ *vs* L titrations (24).

$$E' \overset{K_{iso}}{\rightleftarrows} E + L \overset{K_d}{\rightleftarrows} E \quad (1)$$

$$E_T = E' + E + EL \quad (2)$$

$$E_T = EL/(K_{iso} \cdot K_d \cdot L) + EL/(K_d \cdot L) + EL \quad (3)$$

Which rearranges to,

$$EL = E_T \cdot L/(L + K_d\,(1 + 1/K_{iso})) \quad (4)$$

Alternatively,

$$EL/E_T = \Delta I/\Delta I_{max} = L/(L + K_A). \quad (5)$$

Presteady state binding studies

Binding was monitored by following changes in the intrinsic fluorescence of the enzyme using an Applied Photophysics SX20 stopped-flow spectrometer. Samples were excited at 290 nm, and light emitted above 320 nm was detected using a cutoff filter. Single-mixing experiments involved rapidly mixing (1:1) a solution containing SULT1A1 (0.10 μM), $MgCl_2$ (5.0 mM) and KPO_4 (25 mM, pH 7.4), 25 ± 2 °C with a solution that was identical except that SULT1A1 was replaced with fulvestrant, estradiol or PAPS. Sulfotransferases exhibit a slow, intrinsic hydrolysis of PAPS that must be taken into account in experiments that preincubate PAPS with enzyme, such as the binding of acceptor to the E·PAPS complex. The apparent k_{cat} for SULT1A1 hydrolysis of PAPS was determined using published protocols at saturating ^{35}S-PAPS (7.0 μM) under the conditions of the presteady state experiments ($MgCl_2$ (5.0 mM) and KPO_4 (25 mM, pH 7.4), 25 ± 2 °C), $k_{cat\ (app)}$ = 0.046 min^{-1} (26). To avoid potential complications associate with PAPS hydrolysis, the binding of acceptor to E·PAPS complexes was performed using a two-stage mixing strategy in which PAPS is first mixed with enzyme and binding is allowed to occur for > 5 binding-reaction half-lives before mixing a second time with the acceptor. To measure the binding of estradiol and fulvestrant to SULT1A1·PAPS, a solution containing SULT1A1 (0.20 μM), $MgCl_2$ (5.0 mM) and KPO_4 (25 mM, pH 7.4), 25 ± 2 °C was rapidly mixed (1:1) with a solution lacking SULT1A1 but containing PAPS (400 μM), and the binding reaction was allowed to evolve for 100 msec ($15 \times t_{1/2}$) before mixing a second time (1:1) with a solution containing fulvestrant or estradiol. Reactions were pseudo first order in acceptor concentration in all cases. Typically, binding progress curves were the average of ~ 8 separate pushes. Three progress curves from independently prepared solutions were collected at a given acceptor concentration and averaged. Apparent rate constants were obtained from the averaged data using the Applied Photophysics Pro-Data analysis software

(Marquardt fitting algorithm). Four ligand concentrations were used in constructing k_{obs} *vs* [ligand] plots, from which rate constants were extracted using linear least-squares analysis. The two-stage sequential-mixing experiments were carried out with an SQ.1 sequential-mixing accessory.

Results and Discussion

The gating mechanism

Of the 37 sulfotransferase structures in the PDB, only one is without bound nucleotide, the structure of the SULT2A1·DHEA complex (1J99). Comparison of the nucleotide-free and -bound structures suggests that the opening through which acceptors must pass to enter the active site is substantially constricted by the binding of nucleotide. In an apparent contradiction to the predictions of these structures, substrates too large to pass through the restricted opening are able to bind directly to the E·PAPS complex (30). The affinity of these large substrates decrease 21-fold at saturating PAPS, while the affinities of substrates small enough to pass through the closed pore are not affected by nucleotide. To reconcile the binding and structural studies, it was hypothesized that SULT2A1 isomerizes between open and closed states when nucleotide is bound. This hypothesis, which preserves the spatial restrictions implied by the structures, makes several testable predictions. First, the weakening in the affinity of large substrates will be given by the isomerization equilibrium constant, K_{iso} (see, *Binding algebra*, *Materials and Methods*). Second, the change in affinity caused by nucleotide binding will be due solely to a decrease in the binding on-rate constant because the concentration of the open form (the only form competent to bind large acceptors) is reduced by a factor given by K_{iso}. The experimental validation of these predictions led to the conclusion that the PAPS-bound SULT2A1 isomerizes between open and closed states each with very different acceptor specificities (24).

Gating in-silico

To delve more deeply into the molecular basis of the nucleotide-gated isomerization, the behavior of nucleotide-bound and unliganded enzyme were examined in equilibrium and non-equilibrium molecular dynamics simulations using GROMACS (33). In preparation for the simulations, the structures were equilibrated at 310 °K prior to simulation. The system was considered equilibrated once the all-protein-atom RMSD fluctuations reached a stable value. The approach to equilibrium was exponential and was reached within 5 ns in all cases.

To assess whether the presence of nucleotide determines opening and closure, the system was equilibrated once nucleotide was either removed from the closed- or added to the open-structure. All forms were equilibrated prior to addition or removal of nucleotide. The open or closed status of the structures at simulation end-points were determined entirely by whether or not nucleotide was present. Thus, the *in-silico* system opens and closes in response to nucleotide.

The predicted equilibrium structures and α-carbon dynamics of the open and closed forms of SULT2A1 are presented in Fig 1. The figure has the viewer facing the entrance of the acceptor-binding pocket, which is marked by the small red sphere. The three protein segments that interact to form the opening of the acceptor pocket are highlighted by transparent surfaces. The dynamics (root-mean-squared-fluctuations, RMSF) of the α-carbon backbone are given by the width and color of the chain. Relative to the open structure, the α-carbon fluctuations of the closed (nucleotide-bound complex) are slight and access to the acceptor-binding pocket is quite restricted. As a visual aid in comparing the conformational changes predicted to occur when nucleotide is removed, the transparent surfaces seen in the closed form were superposed onto the open structure. Withdrawing

nucleotide causes the three segments to detach, opening the active-site pore. Segment *one* remains largely in position, *three* unfolds slightly, while *two* undergoes considerable changes in both structure and dynamics. The behaviors predicted by the models mimic the crystallographic data and are well supported by experimental findings (24, 30, 45).

In-silico cap closure

To understand how the cap might close, PAPS was added to the unliganded enzyme *in-silico* and the ensuing cap closure was monitored as a function of time at four conserved positions that are distributed throughout the cap. Each linkage is described in the following paragraph and all are broken as the cap opens. Two of the linkages are located in the "nucleotide half" of the cap, and two are in the "acceptor half." The linkages are shown in Fig 2A and their colors correspond to the traces shown in Panel B. Each trace represents the time-dependence of the distance between moieties whose interactions are broken as the cap opens. Traces were normalized to the average distance in the fully open and closed structures. Each trace is the average of 16 simulations. The absolute distance changes and the atoms used in the measurements are listed in the legend.

Inspection of the PAP-bound structure of SULT2A1 (1EFH (30)) suggests that cap-residue Arg247 (link *one*, Fig 2A) is the only direct contact between the cap and nucleotide. Arg is found at this position in all cytosolic SULTS, and is extensively hydrogen bonded to the 3′-phosphate of PAPS. Link *one* is the earliest to form and appears to initiate cap closure (Fig 2B). Link *two* forms immediately thereafter and stabilizes a cap "kink" that is conserved either as a salt link (SULT2 subfamily) or a π–stacking interaction (SULT1 subfamily). Link *three* is an ionic interaction between the Asp237 carboxylate and the primary ammonium ion of Lys138, and link four is an extensive hydrophobic interaction between cap-residues Leu 233 and 234 and base-residues Trp72, Ile 82 and Phe18. Linkages *three* and *four*, which couple the acceptor section of the cap to the base of the binding pocket, also form together, but well after *one* and *two*. This hysteresis suggests a degree of independence between the two halves of the cap that might allow the acceptor-half to open and close while the donor-half remains shut with nucleotide bound.

While the cap closes in segments, it does not reopen in simulations as long as 20 ns. In an attempt to observe both closure and opening, the stability of the cap was weakened by reducing the charges on the carboxylate oxygens involving the ionic bonds at positions *two* and *three*. Once the charges were reduced to 0.35 eu, the acceptor-half of the cap began to oscillate between open and closed states while nucleotide remained bound in a closed pocket (see, Supplement 1 Movie). Remarkably, the GROMACS models are able to predict not only the nucleotide induced opening and closure of the cap seen in crystallographic data, but an isomerization that explains the gating mechanism and the effects of nucleotide on selectivity.

Gating in the SULT1 Family?

SULT1A1 has the broadest tissue distribution and substrate spectrum of any human cytosolic sulfotransferase (10, 46). The enzyme sulfonates the hydroxyls and primary amines of hundreds, if not thousands, of endo- and xenobiotics. SULT1A1 and 2A1 are similar both in sequence (35% identity, 71% conservation) and structure, yet they differ significantly in regions that define the edge of the acceptor-binding pocket. In particular, SULT1A1 contains a conserved 8-residue proline-rich segment that is not found in SULT2A1 subfamily (Fig 3, *segment 3*; residues 86–93). This seemingly rigid flap is positioned precisely where the pore opens.

To assess the SULT1A1 pore *in-silico*, MD equilibrium simulations of the nucleotide-bound and unliganded forms of the enzyme were performed using GROMACS. At the time this work began there were no published structures of SULT1A1 in complex with PAP. Consequently, the enzyme was co-crystallized with PAP, and the resulting 2.6Å structure (4GRA) was used in our computational models. Since that time, a structure of the binary complex has been published (3U3J (10)). Neither structure uses the canonical dimer interface. Such interfaces are seen in other SULT structures, and this issue has been discussed in detail elsewhere (47, 48). Notably, the monomer structure of 4GRA and 3U3J are virtually identical to 2DO6, which uses the canonical interface (49). The predicted structures and dynamics of nucleotide-bound and unliganded SULT1A1 are presented in Fig 3. The point-of-view is the same as that for the analogous SULT2A1 structures, Fig 1, and the same color-and-width scales was used to represent C_α-chain dynamics. Like SULT2A1, the segments that form the SULT1A1 pore disengage in response to the removal of nucleotide, and the dynamics of the cap (*segment 2*) are predicted to increase substantially as the pore opens. It appears likely that gating occurs in SULT1A1; however, the degree to which gating influences selectivity is determined by the isomerization equilibrium constant, which is not known.

Gating predicts that nucleotide binding will shift the enzyme into the closed form, thus decreasing the concentration of the open form - the only species capable of binding large acceptors. The concentration of the open form decreases to a minimum, non-zero level at saturating PAPS given by the isomerization equilibrium constant, $K_{iso} = [E{\cdot}nuc]_c / [Enuc]_o$, where *c* and *o* refer to *closed* and *open* complexes. In such a mechanism, the affinity of large acceptors for the nucleotide-bound enzyme weakens relative to the free enzyme by an amount given by the Gibbs potential associated with opening the pore (see, *Binding Algebra*, *Materials and Methods*). In contrast, the affinities of small acceptors are not influenced by the nucleotide. The differential effects of nucleotide on the affinities of large and small acceptors are diagnostic for the gating mechanism. Performing this test requires large and small SULT1A1 substrates.

Modeling studies suggested that fulvestrant and estradiol (E2) might be an effective substrate pair (Fig 4) to test gating in SULT1A1. Fulvestrant (Fasodex™), an E2 analogue with a 15-atom, linear R-group at C_7(R) of the B-ring, is a pure antiestrogen used in treating ER-positive tumors that respond poorly to first-line endocrine therapy (50). Both E2 and fulvestrant are SULT1A1 substrates (15, 49). Binding to the E and E·PAP forms of SULT1A1 was assessed in *in-silico* docking experiments using GOLD (43). Structures of unliganded SULTs are not available in the PDB; consequently, E2 and fulvestrant were docked into protein structures generated using GROMACS, as described above. The docking simulations predict that fulvestrant binds the open but not the closed forms of SULT1A1, and that E2 binds similarly to both.

SULT1A1 binary and ternary complexes can be monitored *via* the changes in intrinsic fluorescence (20 – 40%) that occur as ligand binds. Fluorescence change occurs when acceptor binds either to E or E·PAP. Titrations of the E and E·PAP forms of SULT1A1 with E2 and fulvestrant are shown in panels A and B of Fig 5. The affinity of E2 for the open (zero PAP) and closed forms (saturating PAP) are identical within error − 1.7 ± 0.2 μM and 1.9 ± 0.2 μM, respectively. In contrast, the affinity of fulvestrant for the open form (0.28 ± 0.07 μM) is 26-fold greater that its affinity for the nucleotide-bound complex, 6.9 ± 0.9 μM. Thus, at equilibrium and at saturating PAP, only 3.7% of the enzyme is open. The differential effect of PAP on the affinities of E2 and fulvestrant are consistent with the isomerization mechanism.

Antisynergy between PAP and fulvestrant, but not E2, supports gating but can also be explained on the basis of general models of destabilization associated with fulvestrant R-group. Furthermore, the absence of the sulfuryl-moiety of PAPS in the binding studies leads to interpretative ambiguity. To address these uncertainties, a more stringent test of the mechanism was performed. In a simple gating model, nucleotide binding "closes" the gate and thus prevents access to large substrates. The gate occasionally opens with nucleotide bound, allowing substrate to add. Finally, the affinity of the open enzyme for large or small substrates is independent of whether nucleotide is bound. This model predicts that the decrease in affinity of the large substrate caused by the nucleotide is due solely to a decrease in concentration of the open form of the enzyme. Since the rate of ligand binding is a linear function of the concentrations of both ligand and the species to which it binds, the nucleotide should appear to decrease the fulvestrant on-rate constant, and the magnitude of the decrease will be equivalent to the decrease in binding affinity. Furthermore, the fulvestrant off-rate constant will not be affected, since fulvestrant departs from the same form in both cases – the open enzyme. The fulvestrant on-rate constant for the open enzyme does not decrease, it remains fixed; rather, the rate at which fulvestrant binds decreases due to the underlying PAPS-induced decrease in the concentration of ligand-accessible enzyme.

The rate-constants needed to test the gating mechanism were obtained from the slopes and intercepts of k_{obs} *vs* [ligand] plots (51). k_{on} and k_{off} for the binding of fulvestrant and estradiol to SULT1A1 and SULT1A1·PAPS were determined. k_{obs} values were derived from stopped-flow fluorescence, binding-reaction progress curves by least-squares fitting using single-exponential models. A representative progress curve and k_{obs} *vs* [ligand] plot are shown in Figures 6A and B. Ligand concentrations were pseudo-first order and PAPS concentrations were saturating ($29 – 740 \times K_d$). The rate constants are compiled in Table 3.

The E2-binding on- and off-rate constants are not significantly affected by PAPS, and K_d values calculated from the constants agree well with those obtained from the equilibrium-binding measurements. In contrast, the apparent on-rate constant for fulvestrant binding decreases 26-fold at saturating PAPS, which is identical within error to the 28-fold decrease in K_d obtained from the equilibrium-binding measurements. The fulvestrant off-rate constant is not affected by PAPS. These results are precisely those predicted by gating mechanism described above. It appears that SULT1A1, like its sibling SULT2A1, uses a nucleotide-coupled gating mechanism in selecting its substrates.

The utility of the gating mechanism

Sulfotransferases are faced with the challenge of performing two separate but related tasks. They must carry out homeostatic functions that require them to act on a cohort of related structures, and defensive functions in which they sulfonate the myriad compounds that enter through the diet and would otherwise wreak havoc with metabolic signaling systems. The gating mechanism applies a single solution to all large substrates – a gate that can be opened at an energetic price determined by the isomerization equilibrium constant. In this way, evolution need not provide specific structural determinants for each substrate too large to pass through the pore. Indeed, this class of substrates is expected to be extremely diverse, idiosyncratic to the diets and metabolic "set-points" of individuals, and to drift over evolutionary time. Given this diversity, is it questionable whether a static binding site could have achieved a similar end. The concentration of large substrates in hepatocytes will likely increase after feeding, thus the isomerization constant (which is similar for SULTs 1A1 and 2A1) could be "tuned," much in the way that K_m is often set near metabolite concentrations, such that the majority of the enzyme becomes engaged in large-substrate sulfonation only during feeding or under like conditions.

A second advantage of the isomerization mechanism comes into play at very high enzyme concentrations. When the concentration of unliganded enzyme substantially exceeds (> 5 times) substrate dissociation constants, the enzyme partitions according to K_{iso} into two separate high-affinity systems, a closed system that binds small substrates and an open system that predominantly binds large substrates. Under such conditions, it is perhaps best to consider that the substrate becomes saturated with enzyme, rather than the other way around. SULTs 1A1 and 2A1 comprise 0.3% and 0.15%, respectively, of cytosolic protein in human liver (7, 9). In hepatocytes, these SULTs appear to be expressed exclusively in the cytosol (46). One gram wet weight of liver contains ~ 150 mg of cytosolic protein (46, 52, 53) and has a water accessible volume of 0.50 mL (54, 55). These numbers predict that the protein concentration in the hepatocyte cytosol is ~ 300 mg/ml, and that the active-site concentrations of SULTs 1A1 and 2A1 are 24 and 12 μM. These estimates do not take into account that roughly 40% of the cell interior is occupied by organelles (56) that are water accessible and exclude sulfotransferases. These concentrations suggest a > 1 μM reservoir of the open form of SULT1A1 that can act as a high-affinity site for the sulfonation large substrates. It is as if the system is designed to handle low levels of large substrates efficiently, and to buffer its housekeeping functions with an energetic barrier to large-substrate binding.

Conclusions

Consistent with structural data, molecular dynamics simulations predict that the acceptor-binding pocket of SULTs 1A1 and 2A1 open and close in response to the binding of nucleotide. The dynamics of the active-site cap appear to be substantially greater in the open form. The simulations further predict that the acceptor half of the cap oscillates between open and close states while the nucleotide half remains in place with nucleotide bound. This prediction is in complete agreement with the recent report that SULT2A1 isomerizes with nucleotide bound between states that either exclude or admit large substrates, and provides a testable molecular model for the isomerization.

Simulations predict that the acceptor binding pocket of Sult1A1, the most abundant sulfotransferase in human liver, will open and close in response to nucleotide. This hypothesis was tested in equilibrium and presteady-state binding studies using a small/large substrate pair identified in docking studies, fulvestrant and E2. The results clearly demonstrate that the large substrate access to the acceptor-binding pocket is restricted by PAPS binding, while access to small substrates is not affected. The equilibrium constant governing the isomerization when nucleotide is bound is ~ 26, in favor of the closed form. Thus, both SULT1A1 and 2A1, which comprise ~ 90% of the sulfotransferase mass in human liver, use a gating mechanism to select substrates from the complex cytosolic *milieu* in which they perform their vital functions.

Supplementary Material

Refer to Web version on PubMed Central for supplementary material.

Acknowledgments

Supported by the National Institutes of Health Grants GM54469 [1] GM48623[2], and GM38953[3]

Abbreviations

EDTA ethylenediaminetetraacetic acid

E2	estradiol
GSH	glutathione
GST	glutathione S-transferase
HEPES	N-2-hydroxyethylpiperazine-N′-2-ethanesulfonic acid
IPTG	isopropyl β-D-1-thiogalactopyranoside
LB	Luria broth
MBP	maltose binding protein
PAP	3′, 5′-diphosphoadenosine
PAPS	3′-phosphoadinosine 5′-phosphosulfate
PMSF	phenylmethylsulfonyl fluoride
SULT	cytosolic sulfotransferase.

References

1. Falany CN. Enzymology of human cytosolic sulfotransferases. Faseb J. 1997; 11:206–216. [PubMed: 9068609]
2. Bai Q, Xu L, Kakiyama G, Runge-Morris MA, Hylemon PB, Yin L, Pandak WM, Ren S. Sulfation of 25-hydroxycholesterol by SULT2B1b decreases cellular lipids via the LXR/SREBP-1c signaling pathway in human aortic endothelial cells. Atherosclerosis. 2011; 214:350–356. [PubMed: 21146170]
3. Zhang H, Varlamova O, Vargas FM, Falany CN, Leyh TS. Sulfuryl transfer: the catalytic mechanism of human estrogen sulfotransferase. J Biol Chem. 1998; 273:10888–10892. [PubMed: 9556564]
4. Parker CR. Dehydroepiandrosterone and dehydroepiandrosterone sulfate production in the human adrenal during development and aging. Steroids. 1999; 64:640–647. [PubMed: 10503722]
5. Goldstein DS, Swoboda KJ, Miles JM, Coppack SW, Aneman A, Holmes C, Lamensdorf I, Eisenhofer G. Sources and physiological significance of plasma dopamine sulfate. J Clin Endocrinol Metab. 1999; 84:2523–2531. [PubMed: 10404831]
6. Aidoo-Gyamfi K, Cartledge T, Shah K, Ahmed S. Estrone sulfatase and its inhibitors. Anticancer Agents Med Chem. 2009; 9:599–612. [PubMed: 19601744]
7. Riches Z, Stanley EL, Bloomer JC, Coughtrie MW. Quantitative evaluation of the expression and activity of five major sulfotransferases (SULTs) in human tissues: the SULT “pie”. Drug Metab Dispos. 2009; 37:2255–2261. [PubMed: 19679676]
8. Nowell S, Falany CN. Pharmacogenetics of human cytosolic sulfotransferases. Oncogene. 2006; 25:1673–1678. [PubMed: 16550167]
9. Teubner W, Meinl W, Florian S, Kretzschmar M, Glatt H. Identification and localization of soluble sulfotransferases in the human gastrointestinal tract. Biochem J. 2007; 404:207–215. [PubMed: 17335415]
10. Berger I, Guttman C, Amar D, Zarivach R, Aharoni A. The molecular basis for the broad substrate specificity of human sulfotransferase 1A1. PLoS One. 2011; 6:e26794. [PubMed: 22069470]
11. Nishiyama T, Ogura K, Nakano H, Kaku T, Takahashi E, Ohkubo Y, Sekine K, Hiratsuka A, Kadota S, Watabe T. Sulfation of environmental estrogens by cytosolic human sulfotransferases. Drug Metab Pharmacokinet. 2002; 17:221–228. [PubMed: 15618673]
12. Whittemore RM, Pearce LB, Roth JA. Purification and kinetic characterization of a phenol-sulfating form of phenol sulfotransferase from human brain. Arch Biochem Biophys. 1986; 249:464–471. [PubMed: 3463246]

13. Zhang H, Cui D, Wang B, Han YH, Balimane P, Yang Z, Sinz M, Rodrigues AD. Pharmacokinetic drug interactions involving 17alpha-ethinylestradiol: a new look at an old drug. Clin Pharmacokinet. 2007; 46:133–157. [PubMed: 17253885]
14. Glatt H. Sulfotransferases in the bioactivation of xenobiotics. Chem Biol Interact. 2000; 129:141–170. [PubMed: 11154739]
15. Edavana V, Yu X, Dhakal I, Williams S, Ning B, Cook I, Caldwell D, Falany C, Kadlubar S. Sulfation of Fulvestrant by Human Liver Cytosols and Recombinant SULT1A1 and SULT1E1. Pharmacogenomics and Personalized Medicine. 2011; 1:137–145. [PubMed: 22822301]
16. Meinl W, Pabel U, Osterloh-Quiroz M, Hengstler JG, Glatt H. Human sulphotransferases are involved in the activation of aristolochic acids and are expressed in renal target tissue. Int J Cancer. 2006; 118:1090–1097. [PubMed: 16161050]
17. Reiter C, Weinshilboum RM. Acetaminophen and phenol: substrates for both a thermostable and a thermolabile form of human platelet phenol sulfotransferase. J Pharmacol Exp Ther. 1982; 221:43–51. [PubMed: 6950087]
18. Mishiro E, Liu MY, Sakakibara Y, Suiko M, Liu MC. Zebrafish tyrosylprotein sulfotransferase: molecular cloning, expression, and functional characterization. Biochem Cell Biol. 2004; 82:295–303. [PubMed: 15060624]
19. Kurogi K, Chen M, Lee Y, Shi B, Yang T, Liu MY, Sakakibara Y, Suiko M, Liu MC. Sulfation of Buprenorphine, Pentazocine, and Naloxone by Human Cytosolic Sulfotransferases. Drug Metab Lett. 2012
20. Ekuase EJ, Liu Y, Lehmler HJ, Robertson LW, Duffel MW. Structure-activity relationships for hydroxylated polychlorinated biphenyls as inhibitors of the sulfation of dehydroepiandrosterone catalyzed by human hydroxysteroid sulfotransferase SULT2A1. Chem Res Toxicol. 2011; 24:1720–1728. [PubMed: 21913674]
21. Falany JL, Pilloff DE, Leyh TS, Falany CN. Sulfation of raloxifene and 4-hydroxytamoxifen by human cytosolic sulfotransferases. Drug Metab Dispos. 2006; 34:361–368. [PubMed: 16381672]
22. Senggunprai L, Yoshinari K, Yamazoe Y. Selective role of sulfotransferase 2A1 (SULT2A1) in the N-sulfoconjugation of quinolone drugs in humans. Drug Metab Dispos. 2009; 37:1711–1717. [PubMed: 19420132]
23. Falany CN, Wheeler J, Oh TS, Falany JL. Steroid sulfation by expressed human cytosolic sulfotransferases. J Steroid Biochem Mol Biol. 1994; 48:369–375. [PubMed: 8142314]
24. Cook I, Wang T, Falany CN, Leyh TS. A Nucleotide-Gated Molecular Pore Selects Sulfotransferase Substrates. Biochemistry. 2012; 51:5674–83. [PubMed: 22703301]
25. Her C, Kaur GP, Athwal RS, Weinshilboum RM. Human sulfotransferase SULT1C1: cDNA cloning, tissue-specific expression, and chromosomal localization. Genomics. 1997; 41:467–470. [PubMed: 9169148]
26. Sun M, Leyh TS. The human estrogen sulfotransferase: a half-site reactive enzyme. Biochemistry. 2010; 49:4779–4785. [PubMed: 20429582]
27. Minor W, Cymborowski M, Otwinowski Z, Chruszcz M. HKL-3000: the integration of data reduction and structure solution--from diffraction images to an initial model in minutes. Acta Crystallogr D Biol Crystallogr. 2006; 62:859–866. [PubMed: 16855301]
28. Murshudov GN, Vagin AA, Dodson EJ. Refinement of macromolecular structures by the maximum-likelihood method. Acta Crystallogr D Biol Crystallogr. 1997; 53:240–255. [PubMed: 15299926]
29. Emsley P, Cowtan K. Coot: model-building tools for molecular graphics. Acta Crystallogr D Biol Crystallogr. 2004; 60:2126–2132. [PubMed: 15572765]
30. Pedersen LC, Petrotchenko EV, Negishi M. Crystal structure of SULT2A3, human hydroxysteroid sulfotransferase. FEBS Lett. 2000; 475:61–64. [PubMed: 10854859]
31. Eswar N, Webb B, Marti-Renom MA, Madhusudhan MS, Eramian D, Shen MY, Pieper U, Sali A. Comparative protein structure modeling using Modeller. Curr Protoc Bioinformatics Chapter. 2006; 5(Unit 5.6)
32. Smith PE, Gunsteren WFv. The Viscosity of SPC and SPC/E Water. Computer Physics Communications. 1993; 215:315–318.

33. Van Der Spoel D, Lindahl E, Hess B, Groenhof G, Mark AE, Berendsen HJ. GROMACS: fast, flexible, and free. J Comput Chem. 2005; 26:1701–1718. [PubMed: 16211538]
34. Pedersen LC, Petrotchenko E, Shevtsov S, Negishi M. Crystal structure of the human estrogen sulfotransferase-PAPS complex: evidence for catalytic role of Ser137 in the sulfuryl transfer reaction. J Biol Chem. 2002; 277:17928–17932. [PubMed: 11884392]
35. Wang J, Cieplak P, Kollman P. How Well Does a Restrained Electrostatic Potential (RESP) Model Perform in Calculating Conformational Energies of Organic and Biological Molecules? Journal of Computational Chemistry. 2000; 21:1049–1074.
36. van Gunsteren W, Berendsen H. A leap-frog algorithm for stochastic dynamics. Molecular Simulation. 1988; 1:173–185.
37. Berendsen H, Postma J, DiNola A, Haak J. Molecular dynamics with coupling to an external bath. J Chem Phys. 1984; 81:3684–3690.
38. Berendsen, H. Transport properties computed by linear response through weak coupling to a bath. 1991.
39. Hess B, Henk Bekker H, Herman JC, Berendsen HJC, Fraaije JGEM. LINCS: A linear constraint solver for molecular simulations. Journal of Computational Chemistry. 1998; 18:1463–1472.
40. Humphrey W, Dalke A, Schulten K. VMD: visual molecular dynamics. J Mol Graph. 1996; 14:33–38. 27–38. [PubMed: 8744570]
41. Xavier D, Karl G, Bernhard J, Dieter S, von GW, Alan M. Peptide Folding: When Simulation MeetsExperiment. Angew Chem Int Ed. 1999; 38:236–240.
42. Verdonk ML, Berdini V, Hartshorn MJ, Mooij WT, Murray CW, Taylor RD, Watson P. Virtual screening using protein-ligand docking: avoiding artificial enrichment. J Chem Inf Comput Sci. 2004; 44:793–806. [PubMed: 15154744]
43. Verdonk ML, Chessari G, Cole JC, Hartshorn MJ, Murray CW, Nissink JW, Taylor RD, Taylor R. Modeling water molecules in protein-ligand docking using GOLD. J Med Chem. 2005; 48:6504–6515. [PubMed: 16190776]
44. Teramoto T, Sakakibara Y, Liu MC, Suiko M, Kimura M, Kakuta Y. Snapshot of a Michaelis complex in a sulfuryl transfer reaction: Crystal structure of a mouse sulfotransferase, mSULT1D1, complexed with donor substrate and accepter substrate. Biochem Biophys Res Commun. 2009; 383:83–87. [PubMed: 19344693]
45. Rehse PH, Zhou M, Lin SX. Crystal structure of human dehydroepiandrosterone sulphotransferase in complex with substrate. Biochem J. 2002; 364:165–171. [PubMed: 11988089]
46. Falany CN, Vazquez ME, Heroux JA, Roth JA. Purification and characterization of human liver phenol-sulfating phenol sulfotransferase. Arch Biochem Biophys. 1990; 278:312–318. [PubMed: 2327787]
47. Weitzner B, Meehan T, Xu Q, Dunbrack RL. An unusually small dimer interface is observed in all available crystal structures of cytosolic sulfotransferases. Proteins. 2009; 75:289–295. [PubMed: 19173308]
48. Petrotchenko EV, Pedersen LC, Borchers CH, Tomer KB, Negishi M. The dimerization motif of cytosolic sulfotransferases. FEBS Lett. 2001; 490:39–43. [PubMed: 11172807]
49. Gamage NU, Tsvetanov S, Duggleby RG, McManus ME, Martin JL. The structure of human SULT1A1 crystallized with estradiol. An insight into active site plasticity and substrate inhibition with multi-ring substrates. J Biol Chem. 2005; 280:41482–41486. [PubMed: 16221673]
50. Robertson JF, Harrison M. Fulvestrant: pharmacokinetics and pharmacology. Br J Cancer. 2004; 90(Suppl 1):S7–10. [PubMed: 15094758]
51. Johnson, KA. Transient-state kinetic analysis of enzyme reaction pathways. In: Sigman, DS., editor. The enzymes. 3. Academic Press; New York: 1992. p. 1-61.
52. Wynne HA, Wood P, Herd B, Wright P, Rawlins MD, James OF. The association of age with the activity of alcohol dehydrogenase in human liver. Age Ageing. 1992; 21:417–420. [PubMed: 1471579]
53. Renwick AB, Ball SE, Tredger JM, Price RJ, Walters DG, Kao J, Scatina JA, Lake BG. Inhibition of zaleplon metabolism by cimetidine in the human liver: in vitro studies with subcellular fractions and precision-cut liver slices. Xenobiotica. 2002; 32:849–862. [PubMed: 12419015]

54. Goresky CA. A linear method for determining liver sinusoidal and extravascular volumes. Am J Physiol. 1963; 204:626–640. [PubMed: 13949263]

55. Hallbrucker C, vom Dahl S, Lang F, Gerok W, Häussinger D. Modification of liver cell volume by insulin and glucagon. Pflugers Arch. 1991; 418:519–521. [PubMed: 1891339]

56. Okanoue T, Ohta M, Ou O, Kachi K, Kagawa K, Yuki T, Okuno T, Takino T, French SW. Relationship of Mallory bodies to intermediate filaments in hepatocytes. A scanning electron microscopy study. Lab Invest. 1985; 53:534–540. [PubMed: 2414564]

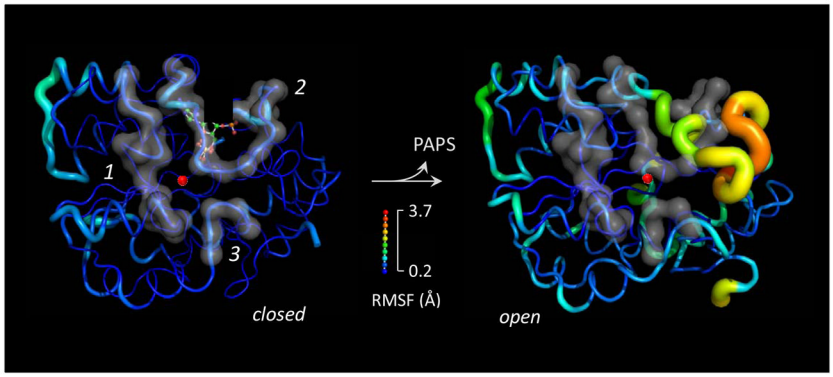

Figure 1. The open and closed forms of SULT2A1in silico

The predicted structures and α-carbon dynamics of SULT2A1 are shown with and without bound nucleotide. The small red sphere marks the entrance of the acceptor-binding pocket. The opening of the acceptor pocket is formed by the three segments (1 – 3) highlighted by transparent surfaces. Segments 1–3 correspond, respectively, to the following residues: Gln67 – Gly83, Asn226 – Gln244, and Thr15 – Arg19. The dynamics (root-mean-squared-fluctuations, RMSF) of the α-carbon backbone are given by the width and color of the chain. As a visual aid, the transparent surfaces seen in the closed state are superposed onto the open structure.

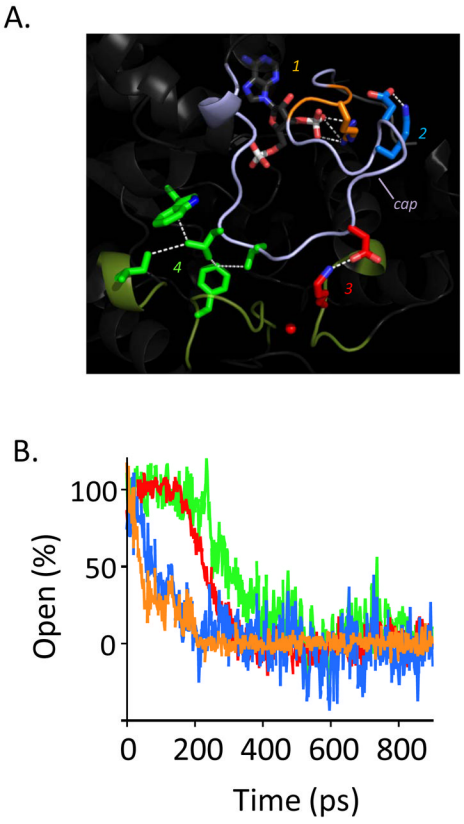

Figure 2. The time dependence of the c ap response to PAPS binding

(A) *Cap linkages selected for non-equilibrium dynamics studies*. Linkages 1–4 are described in the text (see, In-silico cap closure) and highlighted in colors that correspond to those of the traces shown in Panel B. The closed SULT2A1 configuration is shown, and the red sphere indicates the active site point-of-entry for acceptors. (B) *Cap-closure progress curves*. Progress curves show the time-dependence of distances between linkage partners as the cap closes (see, *Panel A*). Closure was induced by adding PAPS to the open SULT2A1 structure at t_0 of simulation. The colors of the traces correspond to the colors of the linkage in Panel A. Progress curves were normalized by plotting the data as percent open. The atoms used in the distance measurements and the maximum distance change associated with each link are as follows: *link 1*, 3′-phosphate phosphorous to Arg 247 N^{δ}, 6.3 Å; *link 2*, Asp241 C^{γ} to Lys242 N^{ϵ}; 4.5 Å; *link 3*, Asp237 C^{γ} to Lys138 N^{ϵ}; 9.1 Å; *link 4*, Leu233 C^{δ} to Ile82 C^{δ}; 4.0 Å.

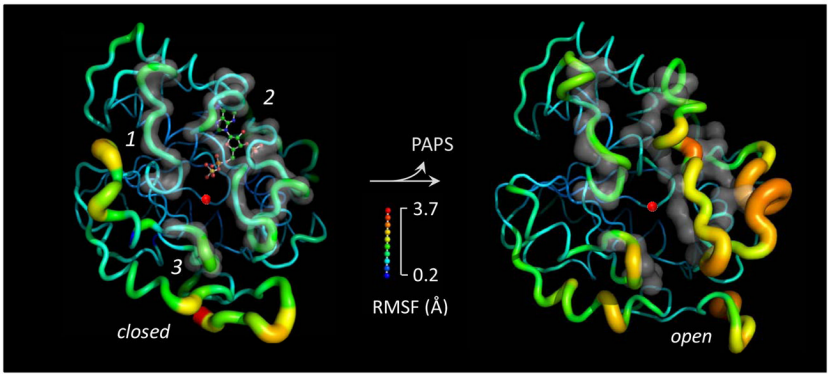

Figure 3. The open and closed forms of SULT1A1 in-silico

The predicted structures and α-carbon dynamics of SULT1A1 are shown with and without bound nucleotide. The entrance of the acceptor-binding pocket is marked by a red sphere. The opening of the pocket is formed by the three segments (1 – 3) highlighted by transparent surfaces. Segments 1–3 correspond, respectively, to the following residus: Asp66 – Met77, Ser228 – Gly259, and Lys85 – Pro90. The dynamics (root-mean-squared-fluctuations, RMSF) of the α-carbon backbone are given by the width and color of the chain. The same width and color scale is used in Figure 1. As a visual aid, the transparent surfaces shown in the closed state are superposed onto the open structure.

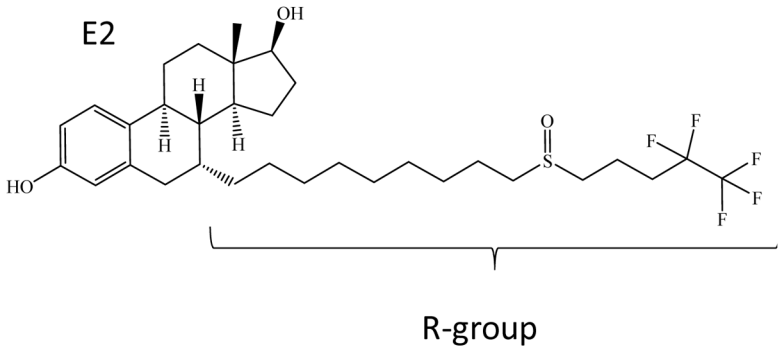

Figure 4. The structure of fulvestrant

Estradiol (E2) provides the steroidal base for the R-group of fulvestrant. Fulvestrant: (7R, 8R,9S,13S,14S,17S)-13-methyl-7-[9-(4,4,5,5,5-pentafluoropentyl-sulfinyl)nonyl]-6,7,8,9,11,12,14,15,16,17,-decahydrocyclopenta[α]phenanthrene-3,17-diol).

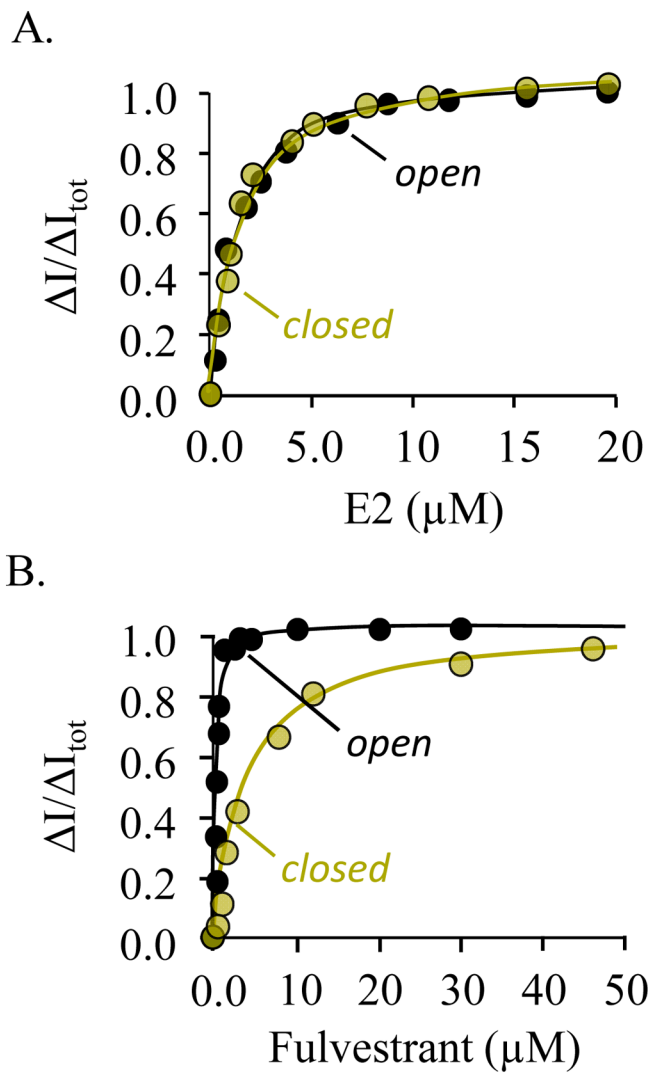

Figure 5. Equilibrium binding of E2 and fulvestrant to the E and E·PAP forms of SULT1A1

(A) *The binding of E2*. E2 binding was monitored *via* changes in intrinsic enzyme fluorescence (λ_{ex} = 290, λ_{em} = 340). Titrant concentrations are given in the figure, the composition of the remainder of the solution was as follows: SULT1A1 (0.050 μM), PAP (0 or 125 μM), $MgCl_2$ (5.0 mM), KPO_4 (25 mM, pH 7.4), 25 ± 2 °C. Fluorescence intensity (ΔI) is normalized to the fluorescence change at saturating ligand (ΔI_{max}). Each point is the average of three independent determinations. The line through the data is the behavior predicted by least-squares fitting using a model that assumes a single-step binding model (see *Materials and Methods*). (B) *The binding of fulvestrant*. Conditions are described in (*A*) except the enzyme concentration was 5.0 nM. Binding constants are compiled in Table 2.

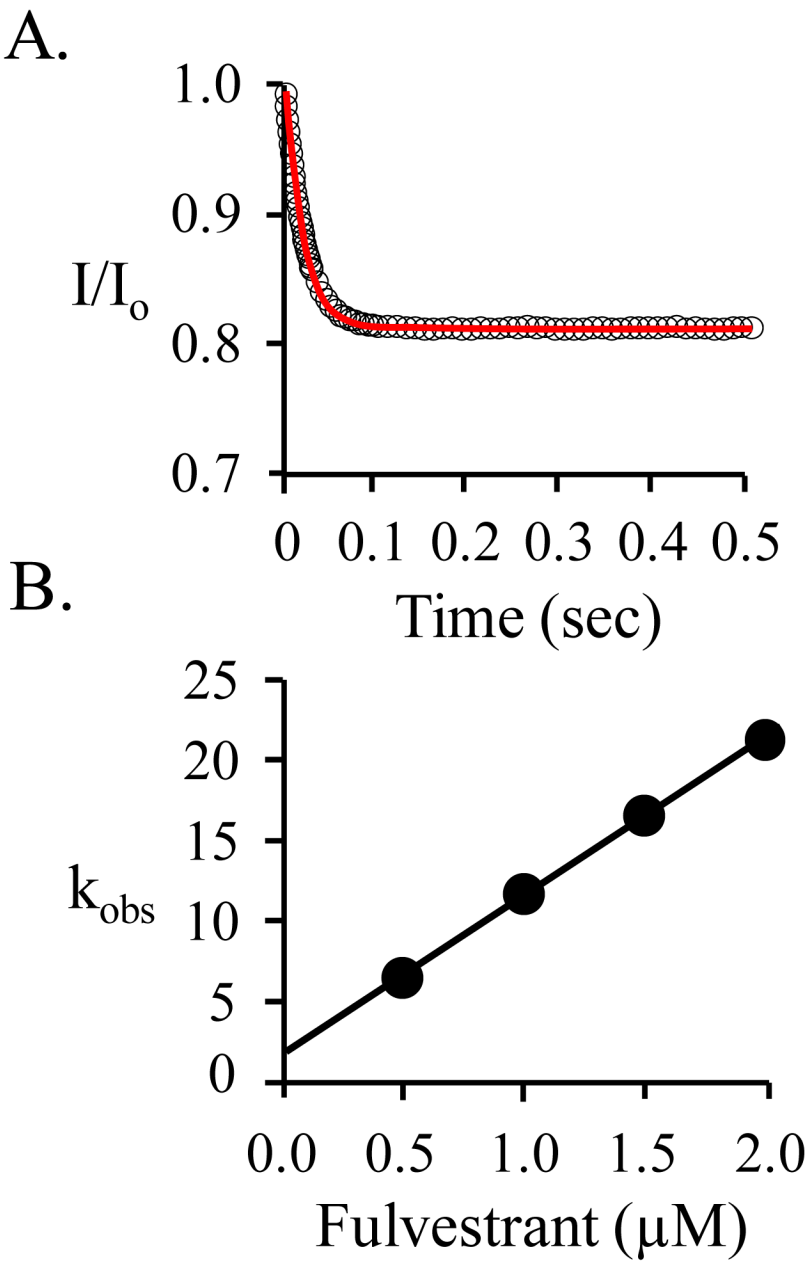

Figure 6. Presteady state binding of fulvestrant to Sult1A1

(A) *Binding of fulvestrant to E.* Binding reactions were initiated by rapidly mixing (1:1) a solution containing fulvestrant (2.0 μM) with a solution containing SULT1A1 (0.05 μM). Binding was monitored by changes in intrinsic enzyme fluorescence (λ_{ex}= 290 nm, and λ_{em} ≥ 330 nm). Fluorescence changes are given relative to the intensity at time zero, I/I_o. Each point represents the average of three independent determinations. The curve through the data represents the behavior predicted by the best fit to a single-exponential model. Conditions: $MgCl_2$ (5.0 mM), K_2PO_4 (25 mM), pH 7.4, T = 25 ± 2 °C. (B) k_{obs} *vs [fulvestrant].* Data were acquired under the conditions describe above and reactions were pseudo-first order in fulvestrant in all cases.

Table 1

Data Collection and Refinement Statistics for the SULT 1A1·PAP Structure

Data Collection	
Space Group	P21
Cell Dimension	
a, b, c (Å)	48.44, 122.63, 55.00
α, β, γ (°)	90.00, 91.46, 90.00
Resolution (Å)	50.0–2.60 [a](2.64–2.60)
I/σ	15.8 (4.5)
Completeness (%)	99.8 (100.0)
Redundancy	6.01 (5.9)
R_{merge}	0.108 (0.355)
Refinement	
Number-of-used-Reflections	16784
Protein Nonhydrogen Atoms	4,649
Ligand Atoms	54
Water Molecules	80
R_{work}	0.214
R_{free}	0.266
RMSD from Ideal Geometry	
Bond Length (Å)	0.008
Bond Angles (°)	1.26

[a]Numbers in parenthesis correspond to the highest resolution shell.

Table 2

SULT1A1 Affinity Constants

Ligand	Enzyme Species	K_d (μM)
E2	^{1} E·	1.7 (0.2)
	PAP·E·	1.9 (0.3)
Ful	E·	0.28 (0.07)
	PAP·E·	7.9 (0.3)

[1] Open-ended dots represent ligand binding sites.

[2] Parentheses enclose standard error estimates.

Table 3

Acceptor-Binding Rate Constants

Ligand	Enzyme Species	k_{on} (M^{-1} s^{-1})	k_{off} s^{-1}	K_d (μM) (k_{off}/k_{on})
E2	[1] E·	[2] 1.6 (0.1) E+06	1.6 (0.2)	1.0 (0.2)
E2	PAPS·E·	1.5 (0.1) E+06	1.9 (0.1)	1.3 (0.1)
Ful	E ·	8.8 (0.2) E+06	1.8 (0.3)	0.27 (0.05)
Ful	PAPS·E ·	2.5 (0.3) E+05	1.7 (0.2)	6.8 (0.9)

[1] Open-ended dots represent ligand binding sites.

[2] Parentheses enclose standard error estimates.